Scale-Invariant Continuous Entanglement Renormalization of a Chern Insulator

Su-Kuan Chu,[1,2] Guanyu Zhu,[1] James R. Garrison,[1,2] Zachary Eldredge,[1,2] Ana Valdés Curiel,[1]
Przemyslaw Bienias,[1] I. B. Spielman,[1] and Alexey V. Gorshkov[1,2]
[1]*Joint Quantum Institute, NIST/University of Maryland, College Park, Maryland 20742, USA*
[2]*Joint Center for Quantum Information and Computer Science, NIST/University of Maryland, College Park, Maryland 20742, USA*

(Received 14 September 2018; published 27 March 2019)

The multiscale entanglement renormalization ansatz (MERA) postulates the existence of quantum circuits that renormalize entanglement in real space at different length scales. Chern insulators, however, cannot have scale-invariant discrete MERA circuits with a finite bond dimension. In this Letter, we show that the continuous MERA (cMERA), a modified version of MERA adapted for field theories, possesses a fixed point wave function with a nonzero Chern number. Additionally, it is well known that reversed MERA circuits can be used to prepare quantum states efficiently in time that scales logarithmically with the size of the system. However, state preparation via MERA typically requires the advent of a full-fledged universal quantum computer. In this Letter, we demonstrate that our cMERA circuit can potentially be realized in existing analog quantum computers, i.e., an ultracold atomic Fermi gas in an optical lattice with light-induced spin-orbit coupling.

DOI: 10.1103/PhysRevLett.122.120502

A quantum many-body system has a Hilbert space whose dimension grows exponentially with system size, making exact diagonalization of its Hamiltonian impractical. Fortunately, tensor networks [1,2] are capable of efficiently representing the ground states of many systems with local interactions [3–8]. Another powerful tool in many-body physics is the renormalization group (RG) [9,10], which uses the fact that the description of a physical system can vary at different length scales, forming a hierarchical structure. The RG provides a systematic prescription to transform an exact microscopic description to an effective coarse-grained description. Applications of RG range from critical phenomena in condensed matter to the electroweak interaction in high-energy physics [11].

One approach, which combines tensor networks and the renormalization group, is called the multiscale entanglement renormalization ansatz (MERA) [3,7]. MERA proposes a quantum circuit acting on a state that is initially entangled at many length scales. The two elementary building-block tensors of the MERA, isometries and disentanglers, are discrete unitary gates that physically implement RG in real space by successively removing entanglement at progressively larger length scales. Interestingly, since the circuit depth only increases logarithmically with the system size, a reversed MERA circuit can efficiently prepare a state with finer entanglement structure from a weakly entangled initial state. In practice, MERAs are most convenient when the disentanglers and isometries are independent of the length scale [12–18]. The state that is left unchanged in the thermodynamic limit by these scale-invariant unitaries is termed a fixed-point wave function.

Experimentally, a reversed MERA circuit might be used to prepare exotic states, such as chiral topological states, which include integer quantum Hall states and certain fractional quantum Hall states [19,20]. Some fractional quantum Hall systems are believed to feature anyons useful for topological quantum computation [21]. Due to their great theoretical interest, it would be useful to be able to study these systems under highly controlled settings, such as in ultracold atomic gases. However, to create a chiral topological state in the lab, we must not only engineer the parent Hamiltonian, but also cool the system down to the ground state. The latter is usually hard experimentally for topological states due to their long-range entanglement [22]. A reversed MERA circuit can possibly resolve this issue by directly generating the target chiral topological state from another state that is easier to obtain by cooling.

Here, as a first step towards finding a MERA for a fractional quantum Hall state, we instead search for a MERA whose fixed-point wave function describes an (integer) Chern insulator. A Chern insulator is an integer quantum Hall state on a lattice and is therefore a simpler system than the fractional quantum Hall state. However, there are no-go theorems stating that a MERA cannot have a Chern insulator ground state as its fixed-point wave function [23–26]. Since conventional MERA only contains strictly local interactions, adding quasilocal interactions with quickly decaying tails could possibly circumvent the no-go theorems. A modified formalism of MERA adapted for field theories called continuous MERA (cMERA) [27] can include such quasilocal interactions [28]. The distinction between strictly local and quasilocal interactions is that the interaction range of the former is finite, while the latter are a broader class that includes interactions decaying faster than any power law with respect to distance, e.g., exponentially decaying interactions. In contrast to the MERA paradigm, in which the renormalization circuit consists of discrete unitary gates, cMERA treats the circuit time, which corresponds to the length scale, as a continuous variable and generates continuous entanglement renormalization using a Hermitian Hamiltonian.

In this Letter, we show that a type of Chern insulator wave function can be generated by a scale-invariant cMERA circuit. The Chern insulator model we consider is the Bernevig-Hughes-Zhang model in the continuum limit [29]. In addition, we propose a possible experimental realization of the cMERA circuit with neutral ^{171}Yb atoms in an optical lattice by introducing spin-orbit coupling.

Our work complements and can be contrasted with Refs. [30,31]. While Ref. [30] previously developed a cMERA for the continuous Chern insulator model mentioned above, our work uses a scale-invariant disentangler. Other prior work in Ref. [31] presented a scale-invariant entanglement renormalization for a two-band Chern insulator model. While Ref. [31] makes use of the lattice structure and quasiadiabatic paths between a series of gapped Hamiltonians, our cMERA approach allows smooth time evolution and emphasizes the continuum physics. Another difference is that the RG evolution in Ref. [31] involves interactions decaying with distance faster than any power-law function but slower than an exponential, whereas our cMERA only needs an exponentially decaying interaction. Other known methods for representing chiral topological states include artificial neural network quantum states [32–34], projected entangled pair states [25,35–37], matrix product states [38], and polynomial-depth unitary circuits [39].

Review of cMERA.—Within the framework of conventional MERA [3,7], disentanglers V_u and isometries W_u are strictly local discrete unitary operators employed to renormalize entanglement at layer $u \in \mathbb{Z}^+$. In cMERA [27], we simply replace them by continuous unitary transformations, which are infinitesimally generated by self-adjoint operators $K(u)$ and L: $V_u \to e^{-iK(u)du}$, $W_u \to e^{-iLdu}$. The notation du denotes an infinitesimal RG step, and $u \in (-\infty, 0]$. When the continuous variable u approaches zero, the system is said to be at the ultraviolet (UV) length scale, possessing both short-range and long-range entanglement. As $u \to -\infty$, the system flows to the infrared (IR) length scale, where short-range entanglement is removed and nearly all degrees of freedom are disentangled from each other. Note that the generator of disentangler $K(u)$ can in general depend on scale u. A cMERA is called scale invariant if $K(u)$ is independent of u.

To emulate the coarse-graining behavior of isometries in conventional lattice MERA, L is chosen to be the scaling transformation in field theory. For example, for a single fermion field $\psi(\mathbf{x})$ in d spatial dimensions, we pick $L = -(i/2)\int[\psi^\dagger(\mathbf{x})\mathbf{x}\cdot\nabla\psi(\mathbf{x}) - \mathbf{x}\cdot\nabla\psi^\dagger(\mathbf{x})\psi(\mathbf{x})]d^d\mathbf{x}$ [27,30]; thereby, fermionic operators $\psi(\mathbf{x})$ in real space and $\psi(\mathbf{k})$ in momentum space satisfy the following scaling transformations: $e^{-iuL}\psi(\mathbf{x})e^{iuL} = e^{(d/2)u}\psi(e^u\mathbf{x})$, $e^{-iuL}\psi(\mathbf{k})e^{iuL} = e^{-(d/2)u}\psi(e^{-u}\mathbf{k})$. One can check that the anticommutation relations $\{\psi(\mathbf{x}), \psi^\dagger(\mathbf{x}')\} = \delta(\mathbf{x}-\mathbf{x}')$ in real space and $\{\psi(\mathbf{k}), \psi^\dagger(\mathbf{k}')\} = \delta(\mathbf{k}-\mathbf{k}')$ in momentum space are preserved under the scaling transformation. We will sometimes abuse the terminology to call $K(u)$ and L themselves the disentangler and the isometry rather than the verbose generator of disentangler and generator of isometry.

The renormalized wave function is governed by the Schrödinger equation,

$$i\frac{\partial}{\partial u}|\Psi^S(u)\rangle = [K(u) + L]|\Psi^S(u)\rangle, \tag{1}$$

where the superscript S denotes the Schrödinger picture. In this Letter, we will focus on the interaction picture, which provides a more convenient way to look at continuous entanglement renormalization. We treat L as a "free" Hamiltonian and $K(u)$ as an "interaction" Hamiltonian, i.e., $|\Psi^I(u)\rangle = e^{iuL}|\Psi^S(u)\rangle$, where the superscript I denotes the interaction picture. Substituting this equation into Eq. (1), we obtain

$$i\frac{\partial}{\partial u}|\Psi^I(u)\rangle = \hat{K}(u)|\Psi^I(u)\rangle, \tag{2}$$

where $\hat{K}(u) \overset{\text{def}}{=} e^{iuL}K(u)e^{-iuL}$ is the disentangler in the interaction picture. The renormalized wave function $|\Psi^I(u)\rangle$ at scale u can be formally written in terms of the IR state $|\Omega^I_{\text{IR}}\rangle \equiv |\Psi^I(u\to-\infty)\rangle$ as

$$|\Psi^I(u)\rangle = \mathcal{P}\exp\left(-i\int_{-\infty}^{u}\hat{K}(u')\mathrm{d}u'\right)|\Omega^I_{\text{IR}}\rangle, \tag{3}$$

where $\mathcal{P}$ is the path ordering operator. Unless otherwise stated, we will only consider the interaction picture; therefore, we will drop the superscript I in the rest of this Letter.

A continuous Chern insulator model.—We begin with a two-band continuous Chern insulator model in two spatial dimensions [29] with Hamiltonian $H = \int d^2\mathbf{k}\psi^\dagger(\mathbf{k})[\mathbf{R}(\mathbf{k})\cdot\boldsymbol{\sigma}]\psi(\mathbf{k})$, where $\mathbf{k} = (k_x, k_y) \in \mathbb{R}^2$, $\mathbf{R}(\mathbf{k}) = (k_x, k_y, m - k^2)$, $m > 0$, $k \equiv |\mathbf{k}| = \sqrt{k_x^2 + k_y^2}$, and $\boldsymbol{\sigma} = (\sigma_x, \sigma_y, \sigma_z)$ is a vector of Pauli matrices. The fermionic operator $\psi(\mathbf{k})$ is a two-component spinor $\psi(\mathbf{k}) \equiv [\psi_1(\mathbf{k})\,\psi_2(\mathbf{k})]^T$ whose components satisfy $\{\psi_i^\dagger(\mathbf{k}),\psi_j(\mathbf{k}')\}=\delta_{ij}\delta(\mathbf{k}-\mathbf{k}')$ for $i,j\in\{1,2\}$.

The ground state, which has the lower band filled, is [30]

$$|\Psi\rangle=\prod_{\mathbf{k}}[u_{\mathbf{k}}\psi_2^\dagger(\mathbf{k})-v_{\mathbf{k}}\psi_1^\dagger(\mathbf{k})]|\mathrm{vac}\rangle,$$
$$u_{\mathbf{k}}=\frac{1}{\sqrt{N_k}}\left[(m-k^2)+\sqrt{(m-k^2)^2+k^2}\right],$$
$$v_{\mathbf{k}}=\frac{1}{\sqrt{N_k}}(ke^{-i\theta_{\mathbf{k}}}), \tag{4}$$

where N_k is a k-dependent normalization factor such that $|u_{\mathbf{k}}|^2+|v_{\mathbf{k}}|^2=1$, and the state $|\mathrm{vac}\rangle$ is the vacuum state annihilated by $\psi_{1,2}(\mathbf{k})$. The angle $\theta_{\mathbf{k}}$ is defined via $k_x=k\cos\theta_{\mathbf{k}}$ and $k_y=k\sin\theta_{\mathbf{k}}$; i.e., it is the polar angle in momentum space. The Chern number of the bottom band of this two-band system is $C=(1/4\pi)\int_{\mathbb{R}^2}d^2\mathbf{k}\mathbf{n}(\mathbf{k})\cdot\{[\partial\mathbf{n}(\mathbf{k})/\partial k_x]\times[\partial\mathbf{n}(\mathbf{k})/\partial k_y]\}=1$, where $\mathbf{n}(\mathbf{k})\equiv[\mathbf{R}(\mathbf{k})/|\mathbf{R}(\mathbf{k})|]$ and where the integrand divided by two is called the Berry curvature.

Now, we show how to obtain a scale-invariant cMERA for this model.

Entanglement renormalization of the Chern insulator.—Following the convention in Refs. [27,30,40], we take the Gaussian ansatz for the disentangler in the Schrödinger picture, $K(u)=i\int d^2\mathbf{k}[g(\mathbf{k},u)\psi_1^\dagger(\mathbf{k})\psi_2(\mathbf{k})+g^*(\mathbf{k},u)\psi_1(\mathbf{k})\psi_2^\dagger(\mathbf{k})]$ [41]. If we require our disentangler to be scale invariant, then $g(\mathbf{k},u)$ should not have explicit u dependence, $g(\mathbf{k},u)=g(\mathbf{k})$. We also take the ansatz that $g(\mathbf{k})=\mathcal{H}(k)e^{-i\theta_{\mathbf{k}}}$, where $\mathcal{H}(k)$ is a real-valued function to be determined. Through rewriting the disentangler as $K(u)=\int d^2\mathbf{k}\psi^\dagger(\mathbf{k})[\mathbf{H}(\mathbf{k})\cdot\boldsymbol{\sigma}]\psi(\mathbf{k})$ with $\mathbf{H}(\mathbf{k})=[\mathcal{H}(k)\sin\theta_{\mathbf{k}},-\mathcal{H}(k)\cos\theta_{\mathbf{k}},0]$, we can intuitively understand its action by imagining an effective magnetic field of strength $\mathcal{H}(k)$ in a clockwise direction about the origin applied to the pseudo-spin at each momentum point. In the interaction picture, the disentangler becomes

$$\hat{K}(u)=i\int d^2\mathbf{k}[\mathcal{H}(e^{-u}k)e^{-i\theta_{\mathbf{k}}}\psi_1^\dagger(\mathbf{k})\psi_2(\mathbf{k})+\mathcal{H}(e^{-u}k)e^{i\theta_{\mathbf{k}}}\psi_1(\mathbf{k})\psi_2^\dagger(\mathbf{k})]. \tag{5}$$

Now, we start to renormalize the wave function and determine the form of the disentangler. We assume that the renormalized wave function at scale u can be expressed as

$$|\Psi(u)\rangle=\prod_{\mathbf{k}}[P_{\mathbf{k}}(u)\psi_2^\dagger(\mathbf{k})-Q_{\mathbf{k}}(u)\psi_1^\dagger(\mathbf{k})]|\mathrm{vac}\rangle, \tag{6}$$

with $|P_{\mathbf{k}}(u)|^2+|Q_{\mathbf{k}}(u)|^2=1$. From Eq. (2), we get

$$P_{\mathbf{k}}(u)=A_{\mathbf{k}}e^{-i\varphi(e^{-u}\mathbf{k})}+B_{\mathbf{k}}e^{i\varphi(e^{-u}\mathbf{k})},$$
$$Q_{\mathbf{k}}(u)=-ie^{-i\theta_{\mathbf{k}}}[A_{\mathbf{k}}e^{-i\varphi(e^{-u}\mathbf{k})}-B_{\mathbf{k}}e^{i\varphi(e^{-u}\mathbf{k})}]. \tag{7}$$

Coefficients $A_{\mathbf{k}}$ and $B_{\mathbf{k}}$ are complex numbers with $|A_{\mathbf{k}}|^2+|B_{\mathbf{k}}|^2=\frac{1}{2}$, and $\varphi(e^{-u}\mathbf{k})\equiv\int_{ke^{-u}}^{\infty}\mathcal{H}(t)(dt/t)$. At UV scale $u=0$, the wave function should match the ground state in Eq. (4); at IR scale $u\to-\infty$, we would like the renormalized wave function to be the product state $\prod_{\mathbf{k}}\psi_1^\dagger(\mathbf{k})|\mathrm{vac}\rangle$ or the product state $\prod_{\mathbf{k}}\psi_2^\dagger(\mathbf{k})|\mathrm{vac}\rangle$ [27,30,40]. By taking $A_{\mathbf{k}}=-(1/2i)$ and $B_{\mathbf{k}}=(1/2i)$, the boundary conditions can be satisfied by requiring

$$\mathcal{H}(k)=\frac{k(m+k^2)}{2[k^4+k^2(1-2m)+m^2]}. \tag{8}$$

Substituting Eq. (8) into Eqs. (6) and (7), we attain an explicit form of the renormalized wave function,

$$|\Psi(u)\rangle=\prod_{\mathbf{k}}\frac{1}{\sqrt{N_{k,u}}}\left[\left((m-k^2e^{-2u})+\sqrt{(m-k^2e^{-2u})^2+k^2e^{-2u}}\right)\psi_2^\dagger(\mathbf{k})-ke^{-u}e^{-i\theta_{\mathbf{k}}}\psi_1^\dagger(\mathbf{k})\right]|\mathrm{vac}\rangle, \tag{9}$$

where $N_{k,u}$ is a normalization factor that depends on k and u. The Berry curvature of the renormalized wave function at different u is shown schematically in Fig. 1. The IR state is $|\Omega_{\mathrm{IR}}\rangle=\lim_{u\to-\infty}|\Psi(u)\rangle=\prod_{\mathbf{k}}e^{-i\theta_{\mathbf{k}}}\psi_1^\dagger(\mathbf{k})|\mathrm{vac}\rangle$, which is equal to $\prod_{\mathbf{k}}\psi_1^\dagger(\mathbf{k})|\mathrm{vac}\rangle=\prod_{\mathbf{x}}\psi_1^\dagger(\mathbf{x})|\mathrm{vac}\rangle$ up to an overall phase. Note that the nonzero Chern number does not survive in the IR state because the integration operation does not commute with the limit $u\to-\infty$. However, at any finite u, the Chern number is always one. Therefore, there is no phase transition during the entanglement

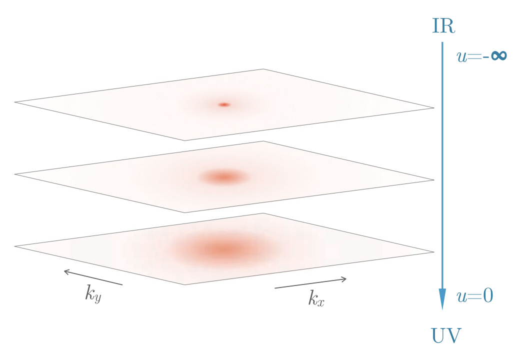

FIG. 1. Berry curvature of the renormalized wave function in the interaction picture at different scales u, drawn schematically in momentum space. The blue arrow corresponds to the direction of the reversed cMERA circuit. The area contributing to the Chern number expands as one approaches the UV scale.

renormalization process, which is consistent with the results in Refs. [30,42,43].

To analyze the spatial structure of the disentangler, we rewrite the expression for $\mathcal{H}(k)$. We first define λ_+ and λ_- as the two roots of the equation $x^2 + (1-2m)x + m^2 = 0$, $\lambda_\pm = [(-1+2m \pm \sqrt{1-4m})/2]$. They are real and negative when $0 < m < 1/4$. Although setting this restriction on m is not necessary for our disentangler, we will assume it in the following in order to assist our experimental realization. Now, the expression $\mathcal{H}(k)$ can be rewritten as

$$\mathcal{H}(k) = \left(\frac{-1+\sqrt{1-4m}}{4\sqrt{1-4m}}\right)\frac{k}{k^2-\lambda_+} + \left(\frac{1+\sqrt{1-4m}}{4\sqrt{1-4m}}\right)\frac{k}{k^2-\lambda_-}. \quad (10)$$

By inserting this expression into Eq. (5) and performing a Fourier transform, it can be shown that the disentangler in real space decays exponentially with characteristic length $e^{-u}/\max\{\sqrt{-\lambda_+}, \sqrt{-\lambda_-}\}$. Therefore, our cMERA involves quasilocal interactions.

Experimental realization of the cMERA circuit.—We propose a way to realize our reversed cMERA circuit to prepare a Chern insulator state in an optical lattice with neutral ^{171}Yb, which are fermionic atoms with two outer electrons. From now on, we will drop the word "reversed" for our cMERA circuit when the context is clear. Recall that the cMERA circuit starts with an initial IR state. As discussed above, the IR state at $u \to -\infty$ does not have the correct Chern number; therefore, we start from a near-IR state with large negative u. In addition, the cMERA circuit is only valid on a lattice when the continuum approximation holds. Therefore, throughout the circuit, the physical length scale $e^{-u}/\max\{\sqrt{-\lambda_+}, \sqrt{-\lambda_-}\}$ should be significantly larger than the lattice spacing. At the same time, this length scale should be significantly smaller than the total size of the lattice so that boundary effects do not dominate the bulk physics. Going forward, we begin with a near-IR state and use our cMERA circuit to obtain the UV state without ever violating these requirements.

Here, we assume that we already have an initial near-IR state waiting to be inserted into the cMERA circuit. Since, in finite-size systems, the Berry curvature is concentrated on a few discrete momentum points near $k=0$, the preparation of this near-IR state should be fast if we can individually create states at each point in momentum space. In the Supplemental Material [44], we provide one possible method for generating this initial state [44].

We now present the cMERA circuit engineering scheme (see Supplemental Material [44] for details). We use $|g_1\rangle$ and $|g_2\rangle$ as shorthand notations for the two stable hyperfine ground states $|F=1/2, m_F=-1/2\rangle$ and $|F=1/2, m_F=1/2\rangle$ in $^1\mathrm{S}_0$; these form the basis of our spinor $\psi(\mathbf{k}) \equiv [\psi_1(\mathbf{k})\,\psi_2(\mathbf{k})]^T$. We find that if we have two

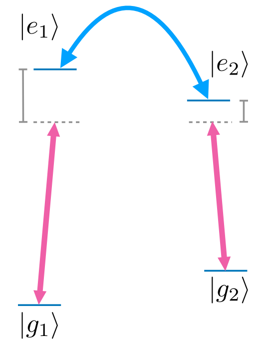

FIG. 2. A scheme to engineer the cMERA circuit in the interaction picture. The two excited states are coupled by spin-orbit interaction to each other and by off-resonant lasers to the two ground states.

metastable excited states $|e_1\rangle$ and $|e_2\rangle$ (e.g., from the ^3P manifold) with quadratic dispersions coupled by spin-orbit interaction and couple them off resonantly to the respective ground states as shown in Fig. 2, then the disentangler in the interaction picture can be engineered. Intuitively, the spin-orbit interaction allows us to generate a momentum-dependent effective magnetic field for Eq. (5), whereas the off-resonant couplings to quadratic dispersive bands induce quadratic terms in the denominators of Eq. (10). To accomplish this, we utilize the scheme detailed in Refs. [53–56] to create two dressed excited states coupled by spin-orbit interaction. However, as the two dressed states are linear combinations of bare excited states, the dressed states do not have good quantum numbers to have clear selection rules to forbid the transitions $|g_1\rangle \leftrightarrow |e_2\rangle$ and $|g_2\rangle \leftrightarrow |e_1\rangle$. Nevertheless, by carefully choosing the driving fields to couple ground states to the bare excited states, we can create interferences to generate synthetic selection rules. By varying the laser parameters as the circuit progresses, we can engineer the disentangler in the interaction picture.

When the UV state is generated by the cMERA circuit, one can then use the experimental techniques introduced in Refs. [57–59] to measure the Chern number and the Berry curvature.

Discussion.—In this Letter, we found a quasilocal cMERA whose fixed-point wave function is a Chern insulator. This is a novel and unexpected way to represent systems with chiral topological order. We also demonstrate that our quasilocal quantum circuit can be realized experimentally in a cold atom system, despite the common intuition that a quantum circuit should be strictly local to allow easier implementation.

In our realization, we only explored one possibility to engineer spin-orbit coupling, but it may be possible to engineer the interaction in other ways, such as using magnetic fields on a chip [60] or microwaves [61]. Other alkaline-earth atoms could also provide promising experimental platforms. Although our experimental realization took place in the interaction picture, one could in principle instead use the Schrödinger picture for cMERA, where the lattice constant must continuously contract in an experiment [62,63]. By using our cMERA circuit, the Chern insulator bulk wave function can be prepared and detected. We leave it for future work to study the edge physics, for which one also needs to apply some unitaries on the edge during the initial state preparation process and to carefully design the corresponding disentanglers; otherwise, the edge physics might not be preserved under the bulk unitary process [42,43,64].

It is also interesting that the Chern insulator ground state is a fixed point of our cMERA with *finite* correlation length. This observation seems to contradict the usual intuition that the fixed point correlation length must be zero or infinity, as the correlation length must decrease under rescaling of each strictly local RG step in real space. However, since our cMERA involves continuous time evolution and quasilocal interactions, it has the potential to restore the original correlation length after a finite time evolution. The no-go theorems in Refs. [23–26] are similarly circumvented by a cMERA construction. Our work suggests that quasilocal RG transformations are a more powerful framework than strictly local RG transformations. It also might shed light on some of the key properties of MERA-like formalisms for a wide range of chiral topological states. In the future, we hope to extend the methods of this Letter to fractional quantum Hall states.

We are grateful to Bela Bauer, Yu-Ting Chen, Ze-Pei Cian, Ignacio Cirac, Glen Evenbly, Zhexuan Gong, Norbert Schuch, Brian Swingle, Tsz-Chun Tsui, Brayden Ware, and Xueda Wen for helpful discussions. This project is supported by the AFOSR, NSF QIS, ARL CDQI, ARO MURI, ARO, NSF PFC at JQI, and NSF Ideas Lab. S. K. C. partially completed this work during his participation in the long-term workshop "Entanglement in Quantum Systems" held at the Galileo Galilei Institute for Theoretical Physics as well as "Boulder School: Quantum Information," which is supported by the National Science Foundation and the University of Colorado. He is also funded by the ACRI fellowship under the Young Investigator Training Program. G. Z. is also supported by ARO-MURI, YIP-ONR, and NSF CAREER (DMR431753240). J. R. G. acknowledges support from the NIST NRC Research Postdoctoral Associateship Award. Z. E. is supported in part by the ARCS Foundation. I. B. S. and A. V. C. acknowledge the additional support of the AFOSR's Quantum Matter MURI and NIST.

[1] R. Orús, A practical introduction to tensor networks: Matrix product states and projected entangled pair states, Ann. Phys. (Amsterdam) **349**, 117 (2014).

[2] J. C. Bridgeman and C. T. Chubb, Hand-waving and interpretive dance: An introductory course on tensor networks, J. Phys. A **50**, 223001 (2017).

[3] G. Vidal, Class of Quantum Many-Body States That Can Be Efficiently Simulated, Phys. Rev. Lett. **101**, 110501 (2008).

[4] F. Verstraete and J. I. Cirac, Matrix product states represent ground states faithfully, Phys. Rev. B **73**, 094423 (2006).

[5] F. Verstraete, M. M. Wolf, D. Perez-Garcia, and J. I. Cirac, Criticality, the Area Law, and the Computational Power of Projected Entangled Pair States, Phys. Rev. Lett. **96**, 220601 (2006).

[6] M. B. Hastings, An area law for one-dimensional quantum systems, J. Stat. Mech. 2007, P08024.

[7] G. Vidal, Entanglement Renormalization, Phys. Rev. Lett. **99**, 220405 (2007).

[8] M. M. Wolf, F. Verstraete, M. B. Hastings, and J. I. Cirac, Area Laws in Quantum Systems: Mutual Information and Correlations, Phys. Rev. Lett. **100**, 070502 (2008).

[9] K. G. Wilson, The renormalization group and the ϵ expansion, Phys. Rep. **12**, 75 (1974).

[10] K. G. Wilson, The renormalization group: Critical phenomena and the Kondo problem, Rev. Mod. Phys. **47**, 773 (1975).

[11] J. Zinn-Justin, *Phase Transitions and Renormalization Group* (Oxford University Press, Oxford, 2007).

[12] M. Aguado and G. Vidal, Entanglement Renormalization and Topological Order, Phys. Rev. Lett. **100**, 070404 (2008).

[13] R. N. C. Pfeifer, G. Evenbly, and G. Vidal, Entanglement renormalization, scale invariance, and quantum criticality, Phys. Rev. A **79**, 040301 (2009).

[14] R. König, B. W. Reichardt, and G. Vidal, Exact entanglement renormalization for string-net models, Phys. Rev. B **79**, 195123 (2009).

[15] R. König and E. Bilgin, Anyonic entanglement renormalization, Phys. Rev. B **82**, 125118 (2010).

[16] S. Singh and G. Vidal, Symmetry-protected entanglement renormalization, Phys. Rev. B **88**, 121108 (2013).

[17] G. Evenbly and S. R. White, Entanglement Renormalization and Wavelets, Phys. Rev. Lett. **116**, 140403 (2016).

[18] J. Haegeman, B. Swingle, M. Walter, J. Cotler, G. Evenbly, and V. B. Scholz, Rigorous Free-Fermion Entanglement Renormalization from Wavelet Theory, Phys. Rev. X **8**, 011003 (2018).

[19] T. H. Hansson, M. Hermanns, S. H. Simon, and S. F. Viefers, Quantum hall physics: Hierarchies and conformal field theory techniques, Rev. Mod. Phys. **89**, 025005 (2017).

[20] X.-G. Wen, Colloquium: Zoo of quantum-topological phases of matter, Rev. Mod. Phys. **89**, 041004 (2017).

[21] C. Nayak, S. H. Simon, A. Stern, M. Freedman, and S. Das Sarma, Non-Abelian anyons and topological quantum computation, Rev. Mod. Phys. **80**, 1083 (2008).

[22] S. Bravyi, M. B. Hastings, and F. Verstraete, Lieb-Robinson Bounds and the Generation of Correlations and Topological Quantum Order, Phys. Rev. Lett. **97**, 050401 (2006).

[23] T. Barthel, M. Kliesch, and J. Eisert, Real-Space Renormalization Yields Finite Correlations, Phys. Rev. Lett. **105**, 010502 (2010).

[24] J. Dubail and N. Read, Tensor network trial states for chiral topological phases in two dimensions and a no-go theorem in any dimension, Phys. Rev. B **92**, 205307 (2015).

[25] T. B. Wahl, H. H. Tu, N. Schuch, and J. I. Cirac, Projected Entangled-Pair States can Describe Chiral Topological States, Phys. Rev. Lett. **111**, 236805 (2013).

[26] Z. Li and R. S. K. Mong, Entanglement renormalization for chiral topological phases, arXiv:1703.00464.

[27] J. Haegeman, T. J. Osborne, H. Verschelde, and F. Verstraete, Entanglement Renormalization for Quantum Fields in Real Space, Phys. Rev. Lett. **110**, 100402 (2013).

[28] Q. Hu and G. Vidal, Spacetime Symmetries and Conformal Data in the Continuous Multiscale Entanglement Renormalization Ansatz, Phys. Rev. Lett. **119**, 010603 (2017).

[29] B. A. Bernevig, T. L. Hughes, and S.-C. Zhang, Quantum spin hall effect and topological phase transition in HgTe quantum wells, Science **314**, 1757 (2006).

[30] X. Wen, G. Y. Cho, P. L. S. Lopes, Y. Gu, X. L. Qi, and S. Ryu, Holographic entanglement renormalization of topological insulators, Phys. Rev. B **94**, 075124 (2016).

[31] B. Swingle and J. McGreevy, Renormalization group constructions of topological quantum liquids and beyond, Phys. Rev. B **93**, 045127 (2016).

[32] Y. Huang and J. E. Moore, Neural network representation of tensor network and chiral states, arXiv:1701.06246.

[33] R. Kaubruegger, L. Pastori, and J. C. Budich, Chiral topological phases from artificial neural networks, Phys. Rev. B **97**, 195136 (2018).

[34] I. Glasser, N. Pancotti, M. August, I. D. Rodriguez, and J. I. Cirac, Neural-Network Quantum States, String-Bond States, and Chiral Topological States, Phys. Rev. X **8**, 011006 (2018).

[35] T. B. Wahl, S. T. Haßler, H. H. Tu, J. I. Cirac, and N. Schuch, Symmetries and boundary theories for chiral projected entangled pair states, Phys. Rev. B **90**, 115133 (2014).

[36] D. Poilblanc, J. I. Cirac, and N. Schuch, Chiral topological spin liquids with projected entangled pair states, Phys. Rev. B **91**, 224431 (2015).

[37] D. Poilblanc, N. Schuch, and I. Affleck, $SU(2)_1$ chiral edge modes of a critical spin liquid, Phys. Rev. B **93**, 174414 (2016).

[38] M. P. Zaletel and R. S. K. Mong, Exact matrix product states for quantum Hall wave functions, Phys. Rev. B **86**, 245305 (2012).

[39] P. Schmoll and R. Orús, Kitaev honeycomb tensor networks: Exact unitary circuits and applications, Phys. Rev. B **95**, 045112 (2017).

[40] M. Nozaki, S. Ryu, and T. Takayanagi, Holographic geometry of entanglement renormalization in quantum field theories, J. High Energy Phys. 10 (2012) 193.

[41] In the cMERA literature, a momentum cutoff Λ is typically provided [27,30]. With a finite cutoff, the UV state generated by a cMERA circuit approximates the ground state of the Hamiltonian up to $O(1/\Lambda)$ corrections. Here, we work in the continuum limit $\Lambda \to \infty$ to avoid this technical subtlety. In principle, these finite-Λ corrections can be worked out explicitly.

[42] M. D. Caio, N. R. Cooper, and M. J. Bhaseen, Quantum Quenches in Chern Insulators, Phys. Rev. Lett. **115**, 236403 (2015).

[43] L. D'Alessio and M. Rigol, Dynamical preparation of floquet chern insulators, Nat. Commun. **6**, 8336 (2015).

[44] See Supplemental Material at http://link.aps.org/supplemental/10.1103/PhysRevLett.122.120502 for details on scale invariance as well as the experimental realization, which includes Refs. [45–52].

[45] T. Fukuhara, A. Kantian, M. Endres, M. Cheneau, P. Schauß, S. Hild, D. Bellem, U. Schollwöck, T. Giamarchi, C. Gross, I. Bloch, and S. Kuhr, Quantum dynamics of a mobile spin impurity, Nat. Phys. **9**, 235 (2013).

[46] F. Nogrette, H. Labuhn, S. Ravets, D. Barredo, L. Béguin, A. Vernier, T. Lahaye, and A. Browaeys, Single-Atom Trapping in Holographic 2d Arrays of Microtraps with Arbitrary Geometries, Phys. Rev. X **4**, 021034 (2014).

[47] X. Zhang, M. Zhou, N. Chen, Q. Gao, C. Han, Y. Yao, P. Xu, S. Li, Y. Xu, Y. Jiang, Z. Bi, L. Ma, and X. Xu, Study on the clock-transition spectrum of cold 171 Yb ytterbium atoms, Laser Phys. Lett. **12**, 025501 (2015).

[48] T. Kohno, M. Yasuda, K. Hosaka, H. Inaba, Y. Nakajima, and F.-L. Hong, One-dimensional optical lattice clock with a fermionic 171 Yb isotope, Appl. Phys. Express **2**, 072501 (2009).

[49] N. D. Lemke, A. D. Ludlow, Z. W. Barber, T. M. Fortier, S. A. Diddams, Y. Jiang, S. R. Jefferts, T. P. Heavner, T. E. Parker, and C. W. Oates, Spin-1/2 Optical Lattice Clock, Phys. Rev. Lett. **103**, 063001 (2009).

[50] C. Y. Park, D.-H. Yu, W.-K. Lee, S. E. Park, E. B. Kim, S. K. Lee, J. W. Cho, T. H. Yoon, J. Mun, S. J. Park, T. Y. Kwon, and S.-B. Lee, Absolute frequency measurement of transition of $^1S_0$ $(F = 1/2) - {}^3P_0(F = 1/2)$ ^{171}Yb atoms in a one-dimensional optical lattice at KRISS, Metrologia **50**, 119 (2013).

[51] A. Yamaguchi, Metastable state of ultracold and quantum degenerate Ytterbium atoms: High-resolution spectroscopy and cold collisions, Ph.D. thesis, Kyoto University, 2008.

[52] U. Busch and K. A. Penson, Tight-binding electrons on open chains: Density distribution and correlations, Phys. Rev. B **36**, 9271 (1987).

[53] D. L. Campbell, G. Juzeliunas, and I. B. Spielman, Realistic Rashba and Dresselhaus spin-orbit coupling for neutral atoms, Phys. Rev. A **84**, 025602 (2011).

[54] D. L. Campbell and I. B. Spielman, Rashba realization: Raman with RF, New J. Phys. **18**, 033035 (2016).

[55] L. Huang, Z. Meng, P. Wang, P. Peng, S.-L. Zhang, L. Chen, D. Li, Q. Zhou, and J. Zhang, Experimental realization of a two-dimensional synthetic spin-orbit coupling in ultracold Fermi gases, Nat. Phys. **12**, 540 (2016).

[56] V. Galitski and I. B. Spielman, Spin-orbit coupling in quantum gases, Nature (London) **494**, 49 (2013).

[57] P. Hauke, M. Lewenstein, and A. Eckardt, Tomography of Band Insulators from Quench Dynamics, Phys. Rev. Lett. **113**, 045303 (2014).

[58] E. Alba, X. Fernandez-Gonzalvo, J. Mur-Petit, J. K. Pachos, and J. J. Garcia-Ripoll, Seeing Topological Order in Time-of-Flight Measurements, Phys. Rev. Lett. **107**, 235301 (2011).

[59] N. Fläschner, B. S. Rem, M. Tarnowski, D. Vogel, D.-S. Lühmann, K. Sengstock, and C. Weitenberg, Experimental reconstruction of the Berry curvature in a Floquet Bloch band, Science **352**, 1091 (2016).

[60] B. M. Anderson, I. B. Spielman, and G. Juzeliunas, Magnetically Generated Spin-Orbit Coupling for Ultracold Atoms, Phys. Rev. Lett. **111**, 125301 (2013).

[61] F. Grusdt, T. Li, I. Bloch, and E. Demler, Tunable spin-orbit coupling for ultracold atoms in two-dimensional optical lattices, Phys. Rev. A **95**, 063617 (2017).

[62] J. H. Huckans, I. B. Spielman, B. L. Tolra, W. D. Phillips, and J. V. Porto, Quantum and classical dynamics of a Bose-Einstein condensate in a large-period optical lattice, Phys. Rev. A **80**, 043609 (2009).

[63] S. Al-Assam, R. A. Williams, and C. J. Foot, Ultracold atoms in an optical lattice with dynamically variable periodicity, Phys. Rev. A **82**, 021604 (2010).

[64] S. Mardanya, U. Bhattacharya, A. Agarwal, and A. Dutta, Dynamics of edge currents in a linearly quenched haldane model, Phys. Rev. B **97**, 115443 (2018).